Metallurgical factors that affect the strand width during continuous casting of DIN 1.4003 stainless steel

by C. Siyasiya*, G.T. van Rooyen and W.E. Stumpf*

Synopsis

One of the problems that is occasionally encountered during the continuous casting of DIN 1.4003 stainless steel (hereafter referred to as 1.4003) is the side bulging effect, a problem that is generally prevalent in ferritic stainless steels. This occurs because the unconstrained narrow sides of the solidification shell are not able to withstand the ferrostatic pressure once the strand has emerged from the mould. Coupled with side bulging, there is strand width variation at high temperatures, i.e. when the steel is in the ferrite-austenite dual phase region. Both of these dimensional changes to the slab profile create some processing problems in subsequent hot rolling operations when unacceptable width variations are encountered.

The strength of the solidification shell and its ability to withstand the ferrostatic pressure during continuous casting is dependent on its thickness and phase composition when exiting from the mould up to a few metres downstream. From the study of the high temperature metallurgical behaviour of this steel, it was observed that a thicker solidification shell when exiting from the mould and a higher austenite volume fraction in the steel would be favourable for the reduction of the side bulging effect during continuous casting. It was also found that as long as the d-ferrite to austenite phase ratio keeps fluctuating due to variations in chemical composition and process control in the dual phase region from cast to cast, the strand width variation problem would probably persist. The remedy to this effect lies in more strict chemical composition and process control during continuous casting of this steel.

The hot ductility experiments revealed that 1.4003 exhibits good hot ductility in the strand straightening temperature range with a minimum of 75 per cent reduction in area and this was attributed to the high volume fraction of ferrite (0.2 to 0.4) in the steel. This would provide a remedy to side bulging by increasing the secondary cooling rate of the strand in order to form a thicker solidification shell without necessarily risking transverse cracking and other surface defects during unbending.

Keywords: side wall bulging, resistance bending moment, applied bending moment, ferrostatic pressure.

Introduction

1.4003 is 11 to 12 per cent chromium steel that exists in the ferrite-austenite dual phase area of the Fe-Cr binary phase diagram at temperatures between 850˚C and 1250˚C, and at temperatures higher than 1250˚C, this steel is generally fully ferritic[1]. 1.4003 stainless steel is produced by Columbus Stainless (Middelburg, South Africa) using the straight mould, curved bow continuous slab caster. In this continuous slab casting process, the molten steel flows from a ladle through a tundish into the mould. The molten steel freezes against the tapered and water-cooled copper mould with nickel coating on the hot faces to form a solid shell. When the solidification shell exits from the mould, it is subjected to ferrostatic pressure exerted by the column of the liquid steel inside the strand. The most vulnerable are the unconstrained side walls (narrow faces) of the strand, hence, the side bulging effect; see Figure 1. Previous studies[2,3] have shown that the solidification shell growth rate of the narrow side walls of the strand is dependent on the mould flux properties, casting speed and mould taper angle, among other factors.

Due to the complexity of the industrial continuous casting operation, it is practically impossible to measure the surface temperatures continuously after exiting from the mould during the continuous casting process. The temperature profile is, therefore, modelled using an energy balance approach that is based on the heat transfer equations using parameters measured from the plant directly or the laboratory. The data that was used in this work was acquired from an online process control computer that was installed with a proprietary software package to model the surface temperature, solidus and liquidus profiles of the strand; see Figure 2. The modelled solidification shell thickness as the strand exits from the mould was compared to one deduced from the equations below[4]. The equations relate the solidifying shell thickness t to the heat flux removed at the surface of the strand:

* *Department of Materials Science and Metallurgical Engineering of the University of Pretoria.*

 SA ISSN 0038–223X/3.00 + 0.00. Paper received Nov. 2004; revised paper received May 2005.

Metallurgical factors that affect the strand width

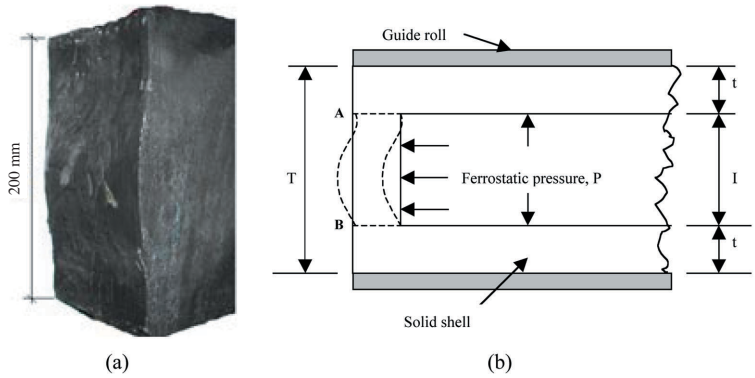

Figure 1—(a) Section of a continuous cast slab for 1.4003 showing side bulging defect on the narrow face of the 200 mm thick continuously cast slab. (b) Schematic presentation of the side bulging of the narrow face of the strand

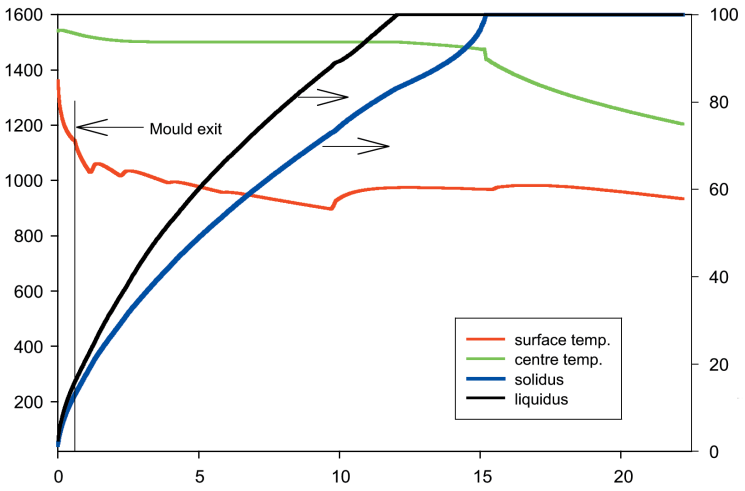

Figure 2—A typical modelled temperature profile for the surface and the centre obtained from an online data acquisition computer during continuous casting of 1.4003

$$t = \frac{\lambda \Delta H_f}{f_q c_p q} + \sqrt{\left(\frac{\lambda \Delta H_f}{f_q c_p q}\right)^2 + \left(\frac{2\lambda L_m}{f_q c_p \rho v_c}\right)} \quad [1]$$

$$f_q = \frac{\alpha L_m e^{-\alpha L_m}}{1 - e^{-\alpha L_m}} \quad [2]$$

$$q = \frac{A v_c^{\beta}}{\alpha L_m}\left(1 - e^{-\alpha L_m}\right) \quad [3]$$

where q is the average heat flux density in W m^{-2}, c_p is the specific heat capacity (representing the enthalpy loss of the solid shell) in J kg^{-1} K^{-1}, ΔH_f is the enthalpy of solidification in J kg^{-1}, L_m is the height of the mould in contact with the strand in m, v_c is the average casting speed in m min^{-1}, f_p is the exponential decrease of the local heat flux density in the casting direction, A is the heat flux density at the meniscus in W m^{-2} (m min^{-1})$^{-0.56}$, α is the slope of the log of heat flux density versus distance from the meniscus in the casting direction in mm^{-1}, β is the slope of log of heat flux density versus the casting speed and ρ is the density of the solid shell in kg m^{-3}.

Applying values and constants determined by Schwerdtfeger *et al.*[4] for a continuous slab caster, i.e. ΔH_f = 262000 J kg^{-1}, c_p = 750 J kg^{-1} K^{-1}, γ = 32 W K-1 m^{-1}, ρ = 7 500 kg m^{-3}, α = 0.0015 mm^{-1}; and for L_m = 0.7 m, β = 0.56, v_c = 1.01 m min^{-1}, the shell thickness as the strand exits from the mould would be 15 mm and from the plant model, it was 14.1 mm. There is, therefore, not much disparity between the two predictions and this validates the continuous casting plant model.

In order to assess the ability of the solidification shell to withstand the ferrostatic pressure during continuous casting, the hot strength of the modelled solidification shell was examined and compared with the plastic bending of the side walls of the solidification shell induced by the ferrostatic pressure.

Previous studies[5,6] have shown that an austenitic solidification shell is generally stronger than a ferritic one and, therefore, it is not surprising that the side bulging problem is more prevalent in ferritic than austenitic stainless steels. Hence, the influence of the chemical composition (additions of austenite formers) on the δ-ferrite to austenite phase change was also investigated.

Experimental techniques

The as-cast 1.4003 with the following chemical composition Fe-0.014C-0.0155N-0.4Ni-0.65Mn-11.28Cr-0.65Si-0.025Ti-0.08V was reheated to 1360°C and soaked for 10 minutes

before being cooled to the tensile test temperature in a Gleeble 1500™ hot working testing machine, simulating the cooling profile during straightening in the continuous caster. The samples were deformed at a strain rate of 2.1 x 10^{-4} s^{-1} that is an order of magnitude higher than the strain rate of 4.62 x 10^{-5} s^{-1} calculated from the continuous caster's parameters. The time to deform the specimen to fracture in the Gleeble at the strain rate in the plant would have been unrealistically long and, therefore, not a reflection of the straightening process itself that lasts for an average of four minutes in the continuous caster. While one set of samples was deformed to fracture (to test hot ductility), the other was deformed to a strain equal to the deformation experienced during straightening, being a true strain of 11.1 x 10^{-3}. The latter was used to assess the influence of deformation on the δ-ferrite to austenite phase transformation by comparing the results with the deformation-free specimens that were given only a furnace heat treatment.

Three chemical compositions of 1.4003 with Kaltenhauser ferrite factors 9.6, 11.5 and 12.1 (see Table I below) were examined for the δ-ferrite to austenite transformation start temperature during continuous cooling. The Kaltenhauser ferrite factor is an empirical expression that is used to predict the microstructure (ferrite volume fraction) at 1000°C, generally in weld metal and is given by[7]:

$$FF = Cr + 6Si + 8Ti + 4Mo + 2Al + 40(C + N) - 2Mn - 4Ni \quad [4]$$

where the chemical compositions are in mass per cent.

Two techniques were used, namely the resistivity method and metallographic analysis. A weld simulator plus resistivity measuring equipment were used in the case of the resistivity method. A computer software program (analySIS) coupled to an optical microscope was used to measure the volume fraction.

Results and discussion

The hot ductility of 1.4003

Results for the hot strength are given in Figures 3, 4 and 5. It is evident from Figure 3 that 1.4003 has good hot ductility with a minimum percentage reduction in area (%RA) of 75 per cent at all of the deformation temperatures tested. Figure 4 is a set of micrographs of the fractured samples exhibiting a typical ductile fracture. Columbus generally experiences no transverse cracking during the continuous casting of 1.4003. This may be attributed to its good hot ductility. As may be seen from Figure 5, the austenite volume fraction increases as the temperature decreases from above 1250°C (the δ-ferrite phase region) and starts regressing to α-ferrite below 1050°C. This is typical of 11–12 per cent chromium steels[8,9]. Extrapolation of the two curves in Figure 5 to zero austenite volume fraction at the upper end, would give the austenite transformation start temperature. It may be concluded that the ferrite volume fraction within the straightening temperature region during continuous casting is about 20 and 40 per cent.

The two curves in Figure 5 are almost identical and, therefore, this suggests that hot deformation does not influence either the δ-ferrite to austenite or the austenite to α-ferrite phase transformation. In other words, the observation that hot deformation does not influence the kinetics of the lower temperature austenite to α-ferrite phase change[9] also holds for the higher temperature δ-ferrite to austenite phase change in 1.4003.

In general (in both the austenitic and ferritic stainless steels), ferrite has good hot ductility properties and is only detrimental when it is present in small amounts as thin films surrounding the austenite grains[10]. The higher volume fraction of ferrite rather than a mere film along the austenite grain boundaries is responsible for the good hot ductility of

Table I

The chemical composition for the 1.4003 steels that were used in the study

Heat No.	C	Mn	Ni	N	Cr	Si	Ti	V	P	S	Mo	Co	FF
3387232	0.018	0.56	0.33	0.021	11.61	0.7	0.032	0.11	0.025	0.003	0.01	0.02	12.1
330011	0.012	0.49	0.55	0.018	11.57	0.38	0.014	0.11	0.027	0.003	0.01	0.02	9.64
3316791	0.021	0.51	0.39	0.018	11.18	0.69	0.033	0.10	0.027	0.002	0.01	0.03	11.5

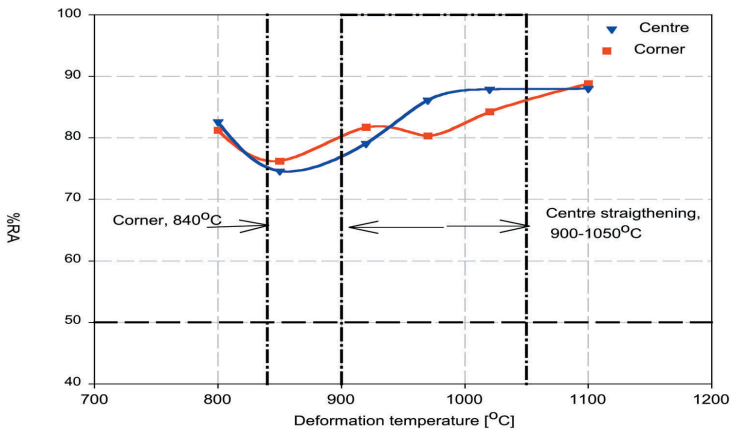

Figure 3—The hot ductility characteristic curves for 1.4003, ferrite factor of 11.36

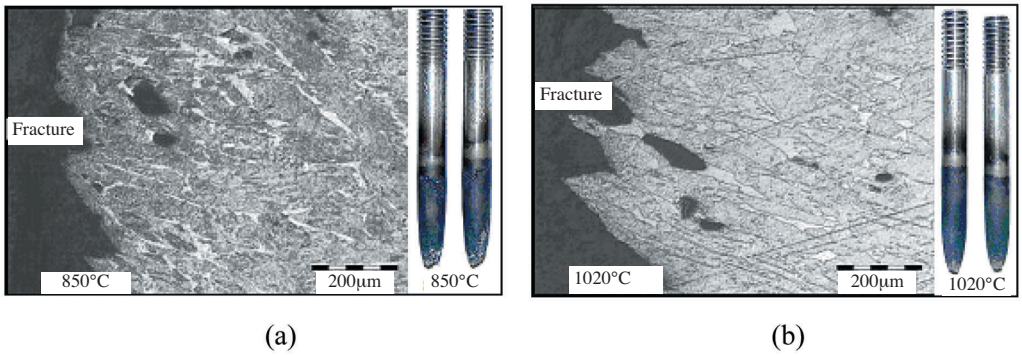

Figure 4—Typical ductile fracture surfaces for 1.4003 (a) at 850°C and (b) at 1020°C

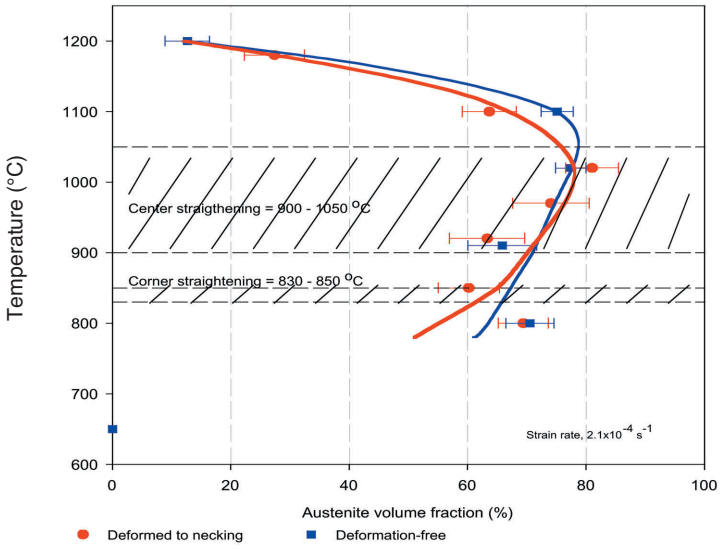

Figure 5—The austenite volume fraction for the deformed and deformation-free samples of 1.4003

1.4003 during continuous casting i.e. there is no strain concentration in the ferrite to cause ductile intergranular failure since the strain is uniformly distributed in the ferrite, Figure 4. Ferrite recovers readily forming serrated grain boundaries that prevents grain boundary sliding[11]. Cardoso *et al.*[12] observed that for high hot ductility in a dual phase steel, the ferrite volume fraction has to approach 40 per cent and 1.4003 seems to meet this condition, at least during the straightening operation in the continuous caster.

The hot strength of 1.4003 and side bulging

Figure 6 shows the steady state flow stress as a function of the testing temperature for 1.4003. This gives an indication of the hot strength of the solidification shell of the strand at a given temperature. The lower strength at high temperatures strengthens the argument that side wall bulging is a high temperature phenomenon, i.e. the strand is most vulnerable to side bulging when it is not only thinnest but also weakest in terms of the solidification shell's ability to withstand the ferrostatic pressure from the liquid column of the steel.

Side bulging can be caused by the ferrostatic pressure of the liquid metal on the relatively thin shell that has to resist the plastic bending to which it is subjected[15]. This implies that side bulging takes place when the resistance bending moment M_R is less than the applied bending moment M_A. For an analysis, the following assumptions were made:

- The ferrostatic pressure exerts a uniformly distributed load on the side walls of the solidifying shell and, therefore, in essence, the unconstrained narrow sides behave like a built-in beam. This is evident from the flat ends of the side bulge, i.e. the side bulge profile in Figure 1 (a).
- The microstructure is homogeneous across the shell thickness at any given temperature.
- The cyclic compressive and tensile strains in the wider face do not affect the strain in the narrow face.
- The uniaxial yield stress (in this case the steady state flow stress) is considered as the yield criterion in analysing the bulging bending moment. The von Mises' yield criterion for a biaxial stress condition can be equated to the uniaxial yield strength with at most a deviation from the former of 15.5 per cent. Furthermore, the longitudinal stress in the casting direction of the strand (due to its own mass) is minimized by the supporting rolls and, therefore, a transverse stress due to ferrostatic force is the main cause of side bulging.

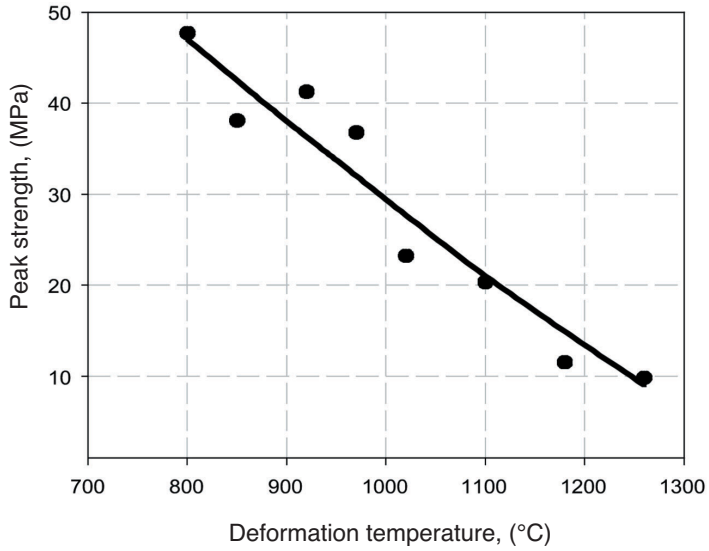

Figure 6—The peak strength (steady state flow stress) variation with temperature for 1.4003 obtained from the Gleeble 1500™

➤ The elastic strain at high temperature is negligible and that creep deformation is governed by the universal hot working equation[13]:

$$A\left(\sinh \beta\sigma_{ss}\right)^{n} = \varepsilon\exp\left(Q/RT\right) = Z \qquad [5]$$

where Q is the activation energy for hot working, R is the universal gas constant which is 8.31 J mol^{-1} K^{-1}, n is the stress sensitivity, T is the absolute temperature, β (MPa^{-1}) is the stress multiplier, Z is the Zener-Hollomon parameter and A is a material constant and σ_{ss} is the steady state flow stress in MPa.

The plastic resistance bending moment M_R provided by the solidification shell would be given by:

$$M_R = \left[\frac{b\sigma_y t^2}{4}\right] \qquad [6]$$

where the yield strength σ_y is replaced by σ_{ss}, t is the shell thickness in metres and b is the unit length along the strand in the casting direction.

Figure 7 was derived from the steady state flow stresses given in Figure 6 and the modelled and schematic shell thicknesses by applying Equation [6]. The resistance bending moment increases almost exponentially along the strand. This is due to the fact that both the strength of the shell as well as the thickness increases as the strand moves downstream. Therefore, side bulging due to ferrostatic pressure is most likely to take place just when the strand exits from the mould, where the bending strength is the least. The ferrostatic pressure P and the plastic bending moment exerted on the narrow sides of the strand (referred to as the applied moment M_A) are given by Equations [7] and [8] respectively.

$$P = g\rho h \qquad [7]$$

$$M_A = \frac{wL^2}{16}\ (\text{built} - \text{in beam}) \qquad [8a]$$

$$M_A = \frac{wL^2}{8}\ (\text{simply supported beam}) \qquad [8b]$$

$$L = T - 2t \qquad [9]$$

where g is the acceleration due to gravity 9.81 m s^{-2}, h is the ferrostatic head in metres, ρ is the density of the liquid steel 6881 kg m^{-3} (taking into consideration the proportions of 87.5 per cent by weight iron and 11.5 per cent chromium and the remaining 1 per cent other alloying elements), the uniformly distributed load w is the ferrostatic pressure P per unit length in N m^{-1} and L is the length AB of the narrow side in m, Figure 1(b) and T is the strand thickness and that is 200 mm.

The ferrostatic pressure is zero at the meniscus of the liquid steel and reaches a maximum value just before the strand fully solidifies. The ferrostatic bending moment increases with ferrostatic head and decreases with the decrease in the length AB as solidification progresses due to the increase in thickness t. As a result, the plastic bending moment reaches a maximum value after which it regresses to zero as the surface area on which it acts diminishes to zero too when the strand is completely solid, Figure 8.

Figure 9 is a comparison of the resistance bending moment M_R offered by the solidification shell with the applied bending moment M_A exerted by the ferrostatic pressure. As may be seen, the strand may be vulnerable to side bulging when M_A is equal to or exceeded M_R, Figure 9 (b). This emphasizes the importance of ensuring that the unconstrained narrow sides of the strand are thick (strong) enough to withstand the ferrostatic pressure as the strand exits from the mould, Figure 9 (c). Many studies in the past[4,14–17] have related the side bulging effect to the interaction of the strand and the mould vis-à-vis heat transfer during continuous casting. Therefore, part of the solution to the problem of bulging lies in the study of the optimization of the cooling rate, mould flux properties, casting speed, mould taper angle, and chemical composition of the steel among other factors.

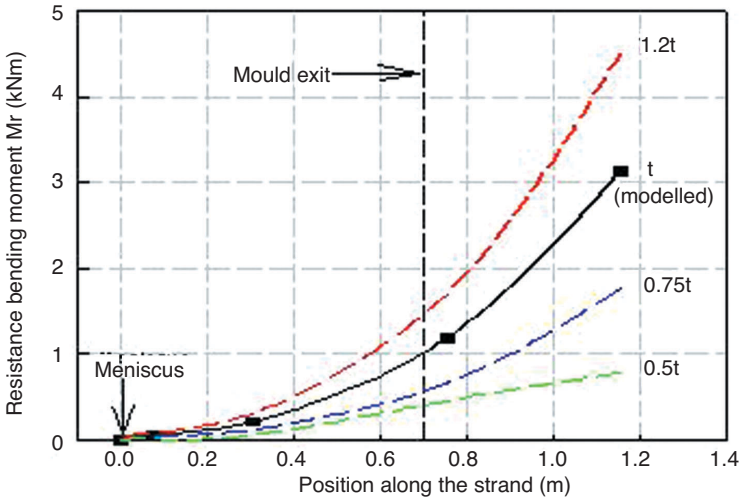

Figure 7—The solidification shell resistance bending moment M_R for the modelled shell thickness curve (solid line) and the schematic thinner and thicker shell thicknesses of *t* (dashed line)

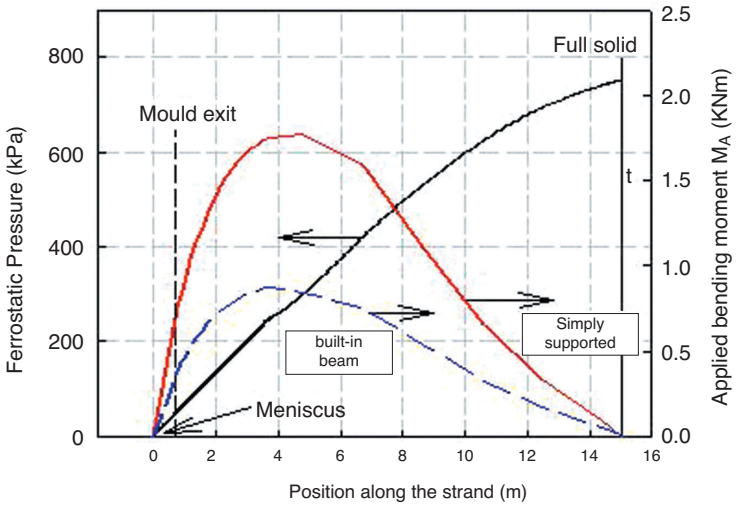

Figure 8—Variation of ferrostatic pressure and the applied bending moment M_A with position along the strand for the built-in beam model (dashed line) and simply supported beam (solid line). The zero position equals the meniscus of the liquid steel in the mould

One of the assumptions that were made in this analysis was that the phase distribution of δ-ferrite and austenite was uniform across the solidification shell thickness. This is not necessarily true because there is a temperature gradient between the outer and inner faces of the solidification shell, the inner face being close to the liquidus. As expected, the inner region of the solidification shell would be fully δ-ferrite while the outer region δ-ferrite plus austenite. The steady state flow stress as a function of temperature, in Figure 6, represents the surface shell strength. This implies that the experimentally determined shell strength could be greater than the actual solidification shell strength during continuous casting.

Effect of chemical composition on the austenite start temperature A_{r5}

Figure 10 shows the experimentally determined continuous cooling transformation (CCT) diagram. It is evident that at cooling rates greater than 60°C/min, the δ-ferrite to austenite phase transformation becomes more sensitive to cooling rate. This suggests that during continuous casting of 1.4003, the δ-ferrite to austenite transformation start temperature is lower on the surface of the strand than at the centre of the strand.

The slab width is measured in the temperature range of 700 to 900˚C (in the δ-ferrite-austenite dual phase region, as may be seen in the CCT diagram) as it exits from the caster and, therefore, the width variation with chemical composition may be ascribed to the ratio of ferrite (BCC) to austenite (FCC) and the cooling rate. Data collected from the continuous caster showed that a higher ferrite factor results in a wider slab width. Hence, it is imperative to stick to stricter chemical composition and process control in order to reduce or avert this width effect.

The results for the effect of chemical composition on the δ-ferrite to austenite transformation start temperature A_{r5} are given in Figure 11. It is evident that austenite transformation from the δ-ferrite starts at earlier times as the ferrite factor decreases, i.e. as the quantity of austenite formers in the steel increases. In fact, the austenite formers do not only shift the

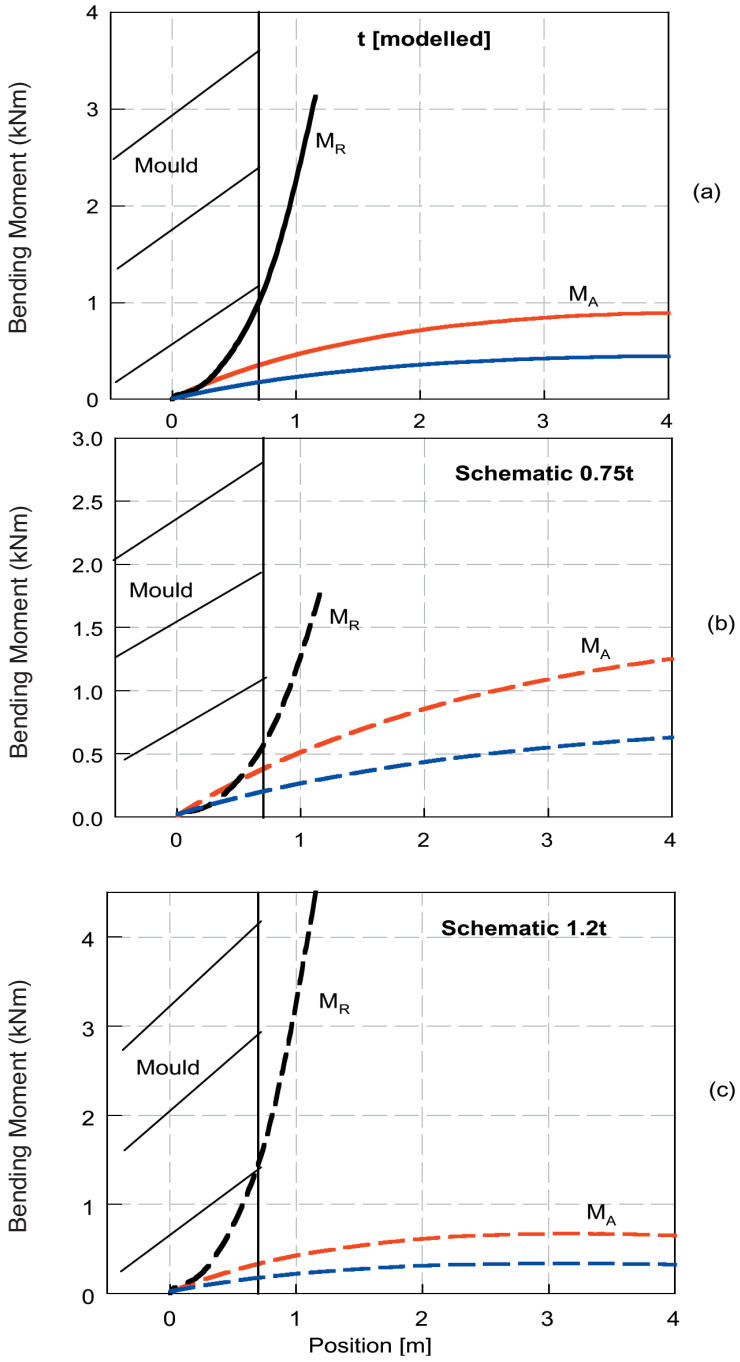

Figure 9—The shell resistance moment M_R and ferrostatic bending moment M_A versus strand position, (a) modelled, (b) and (c) schematic

transformation temperature to earlier times during casting but raise it as well. This is in agreement with previous studies[18] that austenite formers, particularly carbon and nitrogen, enlarge the γ-loop of the iron-chromium equilibrium phase diagram and raise the austenite start temperature A_{r5}. Figure 12 is derived from Figure 11 by plotting the austenite start temperature A_{r5} against the Kaltenhauser ferrite factor at the fastest and slowest cooling rates of 1500 and 30°C/min respectively. The set of micrographs in Figure 13 shows that increasing the quantity of austenite formers (N, C, Ni and Mn) in the steel raises the austenite start temperature A_{r5}. Micrographs in Figure 13 (c) and (d) suggest that the austenite start temperature for the relatively low ferrite factor of 9.64 is somewhere between 1250°C and 1295 °C, i.e. somewhat higher than that of the sample with a ferrite factor of 12.1.

Conclusions

The following conclusions are made from this study:

- The results of this study confirm that the casting conditions within and immediately after the mould need to be optimized to ensure that the solidification shell is thick enough to withstand the ferrostatic pressure exerted on the unconstrained narrow sides of the strand as it exits from the mould. Increasing the cooling rate as one of the significant variables may be

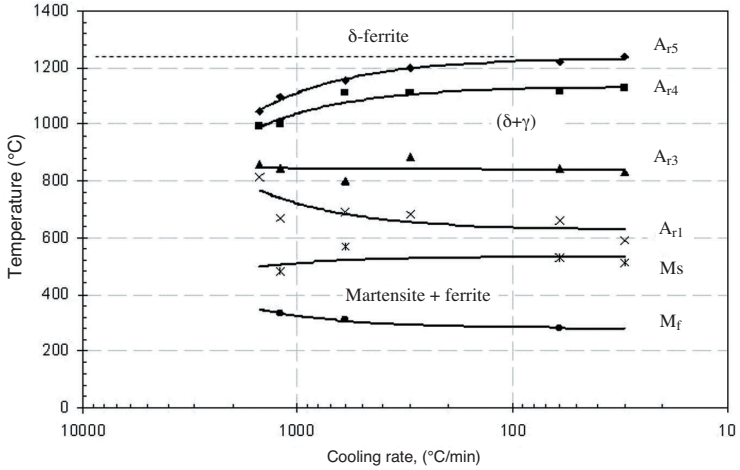

Figure 10—The Continuous Cooling Transformation diagram for 1.4003

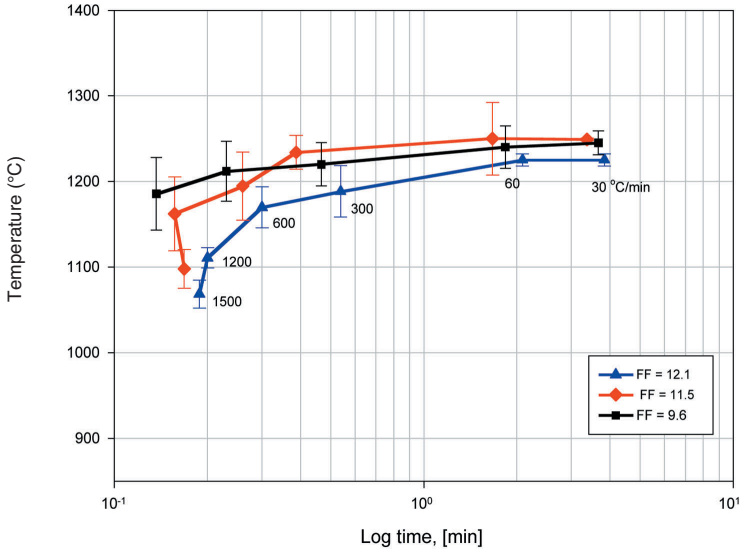

Figure 11—Influence of chemical composition on the measured austenite start temperature A_{r5} for 1.4003 with ferrite factors of 12.1, 11.5, and 9.6

pursued with confidence as this alloy has been shown to have sufficient high temperature ductility during unbending to eliminate the possibility of high temperature cracking.

- Hot deformation appears not to affect the kinetics of either the δ-ferrite to austenite phase transformation or the regression of austenite to α-ferrite under continuous casting conditions of 1.4003 and the transformation kinetics in the undeformed state may be applied with confidence to the strand during unbending.
- Austenite formers (C, N, Ni and Mn) raise the δ-ferrite to austenite transformation start temperature A_{r5} and shift it to earlier transformation start times during continuous casting. Therefore, additions of austenite formers within the 1.4003 specification range may be favourable for a stronger solidification shell since austenite exhibits better hot strength properties than δ-ferrite.
- As long as the δ-ferrite to austenite phase ratio keeps fluctuating due to variations in chemical composition within the specification range and the cooling rate in the dual phase region from cast to cast, the strand width variation effect will probably persist. This is due to the effect of different phase ratios when the strand emerges from the mould.

Acknowledgements

The cooperation, sponsorship, provision of materials and relevant data from Columbus Stainless (Pty) Limited (Middelburg, South Africa) is greatly appreciated. The authors would like also to thank the Materials Science and Metallurgical Engineering Department and IMMRI of the University of Pretoria for the provision of facilities and support that made it possible to carry out this work successfully.

References

1. Baker, H. (ed.) Alloy Phase Diagrams Volume 3, ASM Handbook, 1992 pp. 1.26.
2. Wolf, M.M. Strand Surface Quality of Austenitic Stainless Steels – Part 1: Macroscopic Shell Growth and Ferrite Distribution, *Ironmaking and Steelmaking*, vol. 13, 1986, pp. 248–257.

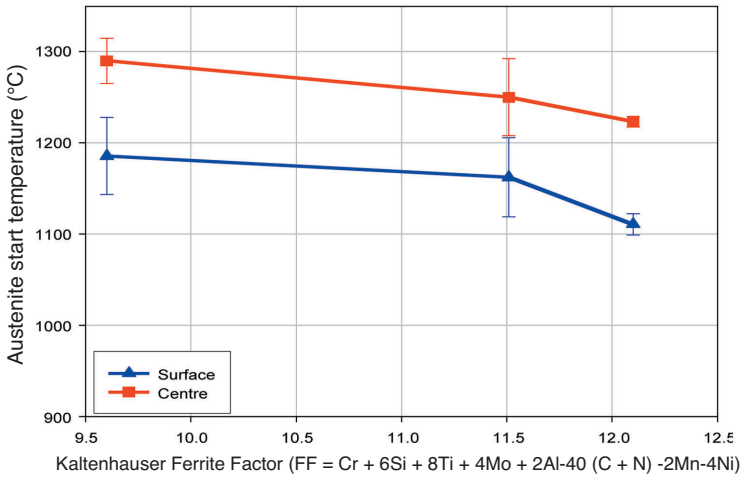

Figure 12—The variation of δ-ferrite to austenite transformation start temperature with chemical composition, expressed as a Kaltenhauser ferrite factor

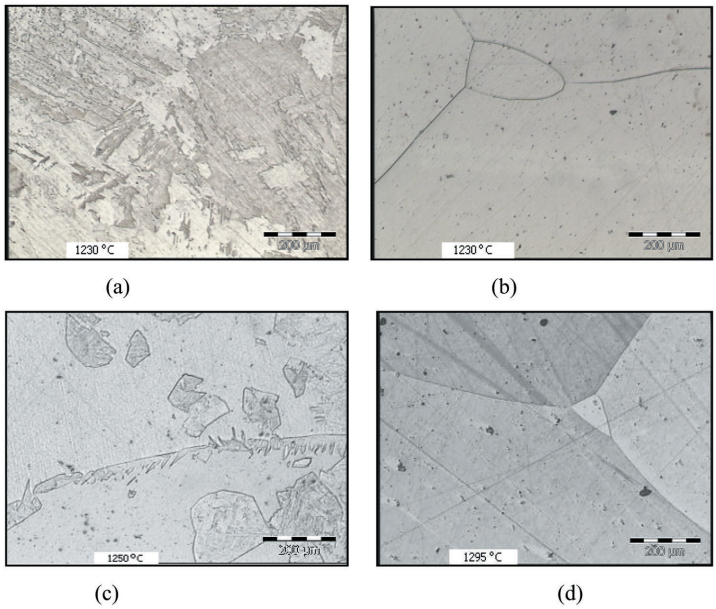

Figure 13—Micrographs for furnace heat treated samples that were solution treated at 1350°C, soaked for 30 minutes, cooled at 1°C/minute and quenched in water from 1230°C: (a) FF=9.64, (b) FF=12.1. (c) and (d) are for FF=9.64 quenched from 1250°C and 1295°C respectively, dark phase is austenite and the light is ferrite

3. Hojo, M. *et al.*, Effect of Mould Powder Properties on the Longitudinal Off-corner Depressions in Continuously Cast SUS304 Slabs *CAMP-ISIJ* 1998, 862.
4. Schwerdtfeder, K.J. Heat Withdraw in Continuous casting of Steel The AISE Steel Foundation, 2003, pp. 1–41.
5. Ray, S.K., Mukhopsdhyay, B., and Das, P.C. Effect of chemistry on solidification and quality of stainless steel, *Annual Tech. Mtg. of India Inst. Metals,* Jamshedpur, Nov. 1999. pp. 14–17.
6. Ray, S.K., Mukhopsdhyay, B., and Bhattacharyya, S.K. Prediction of crack-sensitivity of concast slabs of AISI-430 stainless steel. *ISIJ*, vol. 36, 1996, pp. 611–612.
7. Kaltenhauser R.H. *Met. Eng. Q.*, May 1971, pp. 41–47.
8. Knutsen, R. Influence of compositional banding on grain anisotropy in 3CR12 steel, *Materials Science and Technology*, vol. 7, 1992, pp. 621–627.
9. Zaayman, J.J.J. Improvements to the toughness of the heat affected zone in welds of 11 to 12 per cent chromium steels, PhD thesis, 1994.
10. Mintz, B., Shaker, M., and Crowther, D.N. Hot ductility of an austenitic and a ferritic stainless steel, *Materials Science and Technology*, vol. 13 1997, pp. 243–249.
11. Mintz, B. and Jonas, J.J. Influence of strain rate on production of deformation induced ferrite and hot ductility of steels, *Material Science and Technology*, August 1994, vol. 10, pp. 721–27.
12. Cardoso, G.I.S.L., Mintz, B., and Yue, S. Hot ductility of aluminium and titanium containing steels with and without cyclic temperature oscillations, *Ironmaking and Steelmaking*, 1995, vol. 22, no. 5, pp. 365–377.
13. Zener, C. and Holloman, J.H. *Journal of Applied Physics*, vol. 15, 1944, pp. 22–32.
14. Okimori, M., Fukuda, Y., Tanaka, S., Hojo, M., and Nakano, T. Improvement of Surface Quality of Austenitic Stainless Steel, Nippon Steel Technical Report No. 87 January 2003. pp. 62–66.
15. Irving, W.R. *Continuous Casting of Steel,* First Edition 1993, pp. 8, 59, 150–151.
16. Schrewe, H.F. *Continuous casting of steel*, Verlag Stahleisen mbH, Dusseldorf, 1987.
17. Irving, W.R. and Perkins, A. The Influence of Engineering Process and Chemical Factors on Surface and Internal Quality of Continuous Cast Slabs, International symposium, Durgapur, The Indian Institute of Metals, Oct. 1982, Paper 2.1.
18. Honeycombe, R.W.K. and Bhadeshia, H.K.D.H., *Steels Microstructure and Properties*, 2nd Edition, Edward Arnold, 1995, 252 pp. ◆